Biochemical Pharmacology 168 (2019) 38–47

Contents lists available at ScienceDirect

Biochemical Pharmacology

journal homepage: www.elsevier.com/locate/biochempharm

Pradimicin-IRD exhibits antineoplastic effects by inducing DNA damage in colon cancer cells

Larissa Costa de Almeida[a], Anelize Bauermeister[a,b], Paula Rezende-Teixeira[a], Evelyne Alves dos Santos[c], Luiz Alberto Beraldo de Moraes[b], João Agostinho Machado-Neto[a], Leticia Veras Costa-Lotufo[a,*]

[a] Department of Pharmacology, Institute of Biomedical Sciences, University of São Paulo, São Paulo, Brazil
[b] Faculty of Philosophy, Sciences and Letters of Ribeirão Preto, University of São Paulo, Brazil
[c] Department of Cell Biology and Development, Institute of Biomedical Sciences, University of São Paulo, São Paulo, Brazil

ARTICLE INFO

Keywords:
Natural products
Pradimicin
DNA-damage
DNA-binding
Antitumor agent

ABSTRACT

DNA-damaging agents are widely used in cancer therapy; however, their use is limited by dose-related toxicities, as well as the development of drug resistance. Drug discovery is essential to overcome these limitations and offer novel therapeutic options. In a previous study by our research group, pradimicin-IRD—a new polycyclic antibiotic produced by the actinobacteria *Amycolatopsis* sp.—displayed antimicrobial and potential anticancer activities. In the present study, cytotoxic activity was further confirmed in a panel of five colon cancer, including those with mutation in *TP53* and *KRAS*, the most common ones observed in cancer colon patients. While all tested colon cancer cells were sensitive to pradimicin-IRD treatment with IC_{50} in micromolar range, non-tumor fibroblasts were significantly less sensitive ($p < 0.05$). The cellular and molecular mechanism of action of pradimicin-IRD was then investigated in the colorectal cancer cell line HCT 116. Pradimicin-IRD presented antitumor effects occurring after at least 6 h of exposure. Pradimicin-IRD induced statistically significant DNA damage (γH2AX and p21), apoptosis (PARP1 and caspase 3 cleavage) and cell cycle arrest (reduced Rb phosphorylation, cyclin A and cyclin B expression) markers. In accordance with these results, pradimicin-IRD increased cell populations in the $subG_1$ and G_0/G_1 phases of the cell cycle. Additionally, mass spectrometry analysis indicated that pradimicin-IRD interacted with the DNA double strand. In summary, pradimicin-IRD exhibits multiple antineoplastic activities—including DNA damage, cell cycle arrest, reduction of clonal growth and apoptosis—in the HCT 116 cell line. Furthermore, pradimicin-IRD displays a TP53-independent regulation of p21 expression in HCT 116 *TP53*$^{-/-}$, HT-29, SW480, and Caco-2 cells. This exploratory study identified novel targets for pradimicin-IRD and provided insights for its potential anticancer activity as a DNA-damaging agent.

1. Introduction

DNA integrity is fundamental to cellular functions, including cell proliferation. High-intensity DNA damage promotes the activation of proteins involved in cell cycle checkpoints, leading to cycle arrest to prevent the transmission of genetic errors to daughter cells [1]. The absence of DNA repair results in genetic instability and cell death. Indeed, cancer cells display low detection and repair of DNA damage, which makes them more susceptible to DNA-damaging agents [2,3].

DNA-damage agents are traditionally used in cancer chemotherapy. The clinical use of this class of drugs is limited by their high toxicity and the development of drug resistance. For instance, platinum compounds, which form cross-linked bonds with DNA, have been applied with great success in the treatment of solid tumours: Cisplatin therapy is able to cure more than 90% of all cases of testicular cancer and has good efficacy in the treatment of ovary, bladder, head, neck and cervical cancer [3,4].

Other DNA-damaging drugs include nitrogen mustards (e.g., cyclophosphamide), which act directly by alkylating the DNA in the purine bases, leading to replication arrest and subsequent cell death by apoptosis. Inhibitors of topoisomerase (e.g., doxorubicin) form a DNA-enzyme complex, preventing the re-ligation of DNA strands and causing toxic double-strand breaks. Natural products that lease DNA bases have also been discovered, such as mitomycin C and streptozotocin, which

* Corresponding author at: Department of Pharmacology, Institute of Biomedical Sciences of the University of São Paulo, Av. Prof. Lineu Prestes, 1524, CEP 05508-900 São Paulo, SP, Brazil.
E-mail address: costalotufo@usp.br (L.V. Costa-Lotufo).

https://doi.org/10.1016/j.bcp.2019.06.016
Received 11 March 2019; Accepted 17 June 2019
Available online 19 June 2019
0006-2952/

promote cross-alkylation in double strands of DNA, resulting in a more potent anticancer effect than that provided by single strand alkylation [2–4].

In the context of DNA-damaging natural products, our research group recently described pradimicin-IRD isolated from the actinobacteria *Amycolatopsis* sp. IRD-009 recovered from Brazilian tropical forest soil. Like other compounds of the pradimicin class, the molecular structure of pradimicin-IRD is characterised by an aglycone dihydrobenzo (α) naphthoquinone with glycoside substitutions. However, this unusual pradimicin has a methyl group in the substitution of the D-amino acid and a different aminoglycoside moiety. In the same study, antifungal and cytotoxic activities of pradimicin-IRD were discovered [5]. In the present study, the molecular and cellular effects of pradimicin-IRD as a DNA-damaging agent in the colon cancer cells were further explored.

2. Materials and methods

2.1. Cell culture and inhibitors

HCT 116 (colon adenocarcinoma, ATCC® 247™) cells were obtained from American Tissue and Cell Collection and deposited in the Cell Bank of Rio de Janeiro (Brazil). Professor Bryan Strauss (Cancer Institute of São Paulo State – ICESP) kindly provided HCT 116 *TP53*$^{-/-}$ and HT-29 cells. SW480, Caco-2 cells and primary fibroblast cell culture were kindly provided by Professors Mari Cleide Sogayar (Nucleus of Cellular and Molecular Therapy – Nucel), Silvia Storpirtis (Faculty of Pharmaceutical Sciences – FCF/USP) and Glaucia Santelli (Institute of Biomedical Science – ICB/USP), respectively. Colon cancer cell lines were authenticated by Short Tandem Repeat (STR) matching analysis. Cell culture conditions were developed using the Roswell Park Memorial Institute (RPMI) medium (Thermo Fisher Scientific, San Jose, CA, USA) supplemented with 10% bovine foetal serum (FBS) (Thermo Fisher Scientific, San Jose, CA, USA) and 1% penicillin-streptomycin (Thermo Fisher Scientific, San Jose, CA, USA). Cells were kept in an incubator with 5% CO_2 at 37 °C. Doxorubicin was obtained from Sigma-Aldrich (Sigma-Aldrich, St. Louis, MO, USA). Pradimicin-IRD was produced by *Amycolatopsis* sp. IRD-009 recovered from soil, and the isolation protocol and its structural elucidation were previously published [5]. Dimethyl sulfoxide (DMSO) (Synth, Diadema, SP, Brazil) was used as a vehicle for the dilution of the drugs.

2.2. MTT assay

Cytotoxicity was measured by methylthiazol tetrazolium (MTT) (Thermo Fisher Scientific, San Jose, CA, USA) assay [6]. HCT 116, HCT 116 *TP53*$^{-/-}$, HT-29, SW480, Caco-2 cells and primary fibroblast culture (1×10^4 cells/well) were cultured in a 96-well plate in the RPMI medium, containing 10% FBS and 1% penicillin-streptomycin with increasing concentrations of doxorubicin (0.0032–10 μM) and pradimicin-IRD (0.0032–50 μM) for 72 h. A protocol of intermittent exposure to inhibitors for 6, 12, 24 and 48 h followed by incubation in drug-free media for 72 h was performed using HCT-116 cells, as well as continuous exposure during 24 and 48 h. For time- and dose-response curves, HCT 116 cells were cultured as described above in 96-well plates in the presence of graded concentrations of pradimicin-IRD (0, 0.0032, 0.016, 0.08, 0.4, 2, 10 and 50 μM). DMSO 0.5% was used as a negative control. After treatment, the culture media were replaced with fresh media containing MTT solution (0.5 mg/mL) and incubated for an additional 3 h. Then the MTT solution was removed, and the plates were dried at 35 °C for 30 min. A formazan product was solubilized by 150 μL of DMSO, and the absorbance was obtained at 540 nm. IC_{50} values and their 95% confidence intervals were calculated using sigmoidal nonlinear regression analysis performed with GraphPad Prism 5 (GraphPad Software, Inc., San Diego, CA, USA).

Table 1
Primer sequences and concentrations.

Gene	Sequence	Concentration
BCL2	FW: ATGTGTGTGGAGAGCGTCAA RV: ACAGTTCCACAAAGGCATCC	150 nM
BCL2L1	FW: CTTGGATGGCCACTTACCTGAA RV: GCTGCTGCATTGTTCCCATA	150 nM
MCL1	FW: GTAATAACACCAGTACGGACGG RV: TCCCGAAGGTACCGAGAGAT	150 nM
BAX	FW: GAGCTGCAGAGGATGATTGC RV: CAGCTGCCACTCGGAAAA	150 nM
BAD	FW: CACCAGCAGGAGCAGCCAAC RV: CGACTCCGGATCTCCACAGC	150 nM
BAK1	FW: TGAGTACTTCACCAAGATTGCCA RV: AGTCAGGCCATGCTGGTAGAC	150 nM
CCNA2	FW: GCCTTTCATTTAGCACTCTACA RV: CAGGGTATATCCAGTCTTTCG	300 nM
CCNB1	FW: GTCTCCATTATTGATCGGTTCATG RV: CCAATTTCTGGAGGGTACATTTCT	300 nM
CCND1	FW: CTCGGTGTCCTACTTCAAATG RV: AGCGGTCCAGGTAGTTCAT	300 nM
CCNE1	FW: TATATGGCGACACAAGAAAATG RV: GTGCAACTTTGGAGGATAGA	300 nM
CDKN1A	FW: TGTCACTGTCTTGTACCCTTGT RV: GCCGGCGTTTGGAGTGGTAG	300 nM
CDKN1B	FW: ACTCTGAGGACACGCATTTGGT RV: TCTGTTCTGTTGGCTCTTTTGTT	300 nM
HPRT1	FW: GAACGTCTTGCTCGAGATGTGA RV: TCCAGCAGGTCAGCAAAGAAT	150 nM
ACTB	FW: AGGCCAACCGCGAGAAG RV: ACAGCCTGGATAGCAACGTACA	150 nM

2.3. Trypan blue exclusion

Cell viability was measured using a Trypan blue dye (Sigma-Aldrich, St. Louis, MO, USA) exclusion test after incubation of HCT 116 cells (1×10^5 cells/mL) with pradimicin-IRD at 1.25, 2.5 and 5 μM. Aliquots were removed from cultures after 48 h, and cells that did not display Trypan blue staining were counted in a Neubauer chamber. Doxorubicin (1 μM) was used as a positive control.

2.4. Morphological and immunofluorescence analysis

Morphological changes were analysed via light microscopy (Labomed TCM 400 Inverted, Labo America Inc. Fremont, CA, USA) and by immunofluorescence microscopy (LionHeart FX automated microscope, Biotek, Winooski, VT, USA and Zeiss Fluorescence Microscope, Goeschwitzer, Jena, Germany). In brief, HCT 116 cells (5×10^4 cells/mL) were incubated with doxorubicin 1 μM (positive control) or pradimicin-IRD at 2.5 and 5 μM for 48 h on a circular coverslip inside a 24-well plate, fixed with methanol for 1 min and stained with haematoxylin-eosin (NEWPROV, Pinhais, PR, Brazil). For immunofluorescence analysis, cells were fixed with 3.7% formaldehyde (Sigma-Aldrich, St. Louis, MO, USA) for 30 min, permeabilized with 0.5% Triton-X (Sigma-Aldrich, St. Louis, MO, USA) 100 for 30 min, blocked with 1% BSA for 1 h and labelled with α/β-tubulin (#T5168, #T5293, Sigma-Aldrich, St. Louis, MO, USA) or γH2AX (#9718; Cell Signaling Technology, Danvers, MA, USA) for 16 h, followed by the addition of FITC-labelled anti-rabbit or anti-mouse antibodies (#4412, #4408, Cell Signaling Technology, Danvers, MA, USA) for 2 h. Then the nuclei were stained with DAPI (Thermo Fisher Scientific, San Jose, CA, USA) for 10 min, and the blades were set with a fluorescence-protective solution (anti-fading-Vectashield; Vector Laboratories, Inc. Burlingame, CA, USA), sealed and held at −20 °C and kept away from light sources.

2.5. Clonogenic assay

HCT 116 cells (2×10^3 cells/35 mm^2 plate) were incubated with doxorubicin 1 μM or pradimicin 1.25, 2.5 and 5 μM for 6 h, and then the

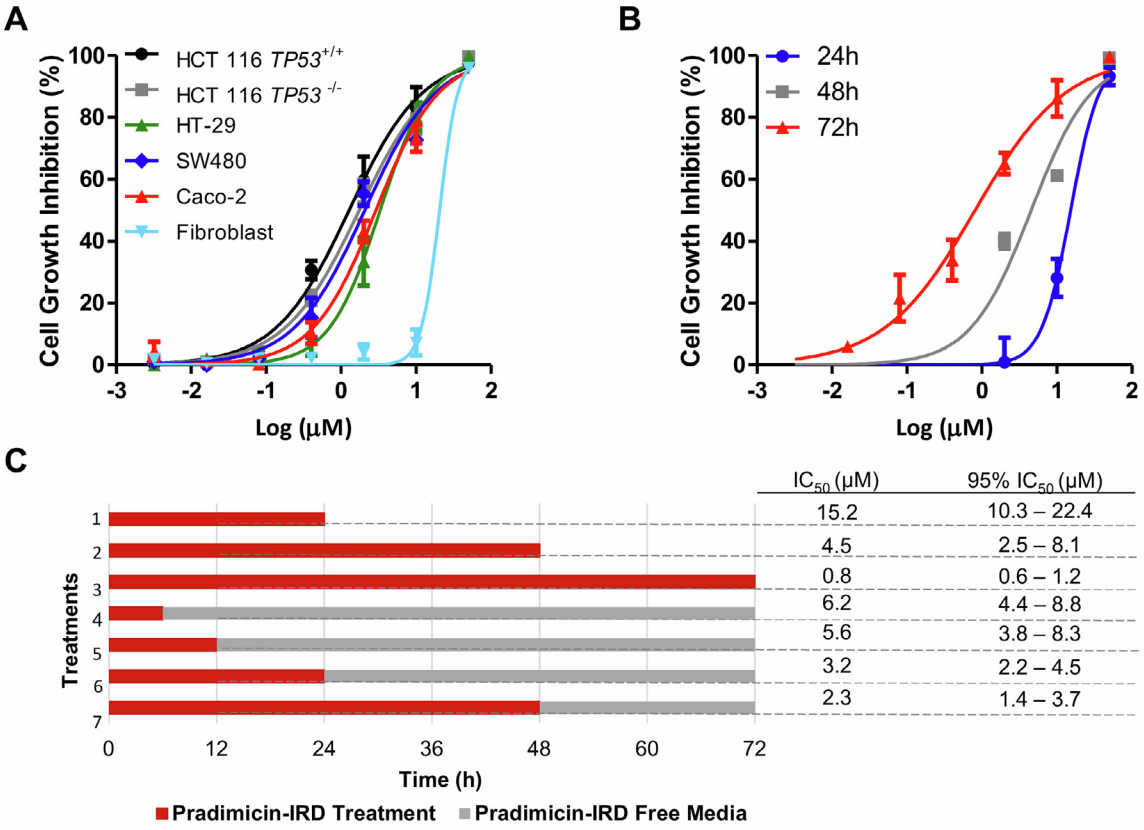

(caption on next page)

Fig. 1. Pradimicin-IRD reduces cell viability and leads to morphological changes in HCT 116 cells. Dose response curves of the cytotoxicity kinetics of pradimicin-IRD after 72 h of treatment in HCT 116, HCT 116 TP53$^{-/-}$, HT-29, SW480 and Caco-2 (n = 3) (mean ± SEM) (A). Dose response curves for pradimicin-IRD treatment during 24, 48 and 72 h in HCT 116 cells (n = 2); values are expressed in terms of mean and standard error of the mean (mean ± SEM) (B). The bar graph indicates the duration of treatment with IRD (red bar) and the time of incubation in a drug-free medium (grey bar); IC_{50} values are described in Figure (C). The percentage of viable HCT 116 cells in the control group (DMSO 0.1%), doxorubicin (1 μM) and pradimicin-IRD treatment groups at 1.25, 2.5 and 5 μM, as indicated by Trypan assay (n = 3) (mean ± SEM); ANOVA, one way, followed by Tukey's multiple comparison test, $^{**}p < 0.001$ $^{***}p < 0.0001$ (D). Haematoxylin and eosin (H&E) staining of HCT 116 cells after 48 h of incubation with DMSO 0.1%, doxorubicin 1 μM, or pradimicin-IRD at 2.5 and 5 μM (400 ×). Arrows indicate condensed chromatin (suggestive of apoptosis) (E). Immunofluorescence of α/β-tubulin and DAPI in HCT 116 cells after 48 h of incubation with DMSO 0.05% and Pradimicin-IRD 5 μM. Arrows indicate condensed chromatin (suggestive of apoptosis) (F). (For interpretation of the references to colour in this figure legend, the reader is referred to the web version of this article.)

Table 2
Mean inhibitory concentration (IC_{50}) of pradimicin-IRD (0.0032–50 μM) in colorectal carcinoma cell lines (HCT 116 *TP53*$^{+/+}$, HCT 116 *TP53*$^{-/-}$, HT-29, SW480, Caco-2) and primary fibroblast cell culture [(n = 3; mean and confidence interval (95%)].

	IC_{50} (μM)	95% IC_{50} (μM)
HCT 116 *TP53*$^{+/+}$	1.28*	0.96–1.70
HCT 116 *TP53*$^{-/-}$	1.74*	1.44–2.11
HT-29	3.32*	2.65–4.16
SW480	2.07*	1.62–2.64
Caco-2	2.91*	2.38–3.55
Fibroblast	20.55	17.20–24.55

*Indicates parameters that are statistically significantly different from those of IC_{50} in primary fibroblast cell culture ($p < 0.0001$).

medium was replaced with a drug-free medium. Colonies were detected after 7 days of culture by adding 1:1 ratio of 0.5% crystal violet solution (Sigma-Aldrich, St. Louis, MO, USA) and methanol (Synth, Diadema, São Paulo, Brazil) 0.5% crystal violet solution and 1:1 methanol. Images were acquired using the G: BOX Chemi XRQ (Syngene, Cambridge, UK) and analysed using ImageJ software (US National Institutes of Health, Bethesda, MD, USA).

2.6. Cell cycle analysis

HCT 116 cells were cultured in the presence of doxorubicin (1 μM) or pradimicin-IRD (1.25, 2.5 and 5 μM) for 24 and 48 h. Cells were then fixed with 70% ethanol (Sigma-Aldrich, St. Louis, MO, USA) for 1 h and incubated for 30 min with staining solution (0.1% Triton-X 100, 0.1 mg/mL of RNAse (Merck, Darmstadt, Hessen, Germany) and 1 μg/mL of propidium iodide (Sigma-Aldrich, St. Louis, MO, USA). DNA content distribution was acquired in a FACSCalibur cytometer (Becton Dickinson, Lincoln Park, NJ, USA), and the data were analysed using FlowJo software (Treestar, Inc., San Carlos, CA, USA).

2.7. Apoptosis assay

HCT 116 cells were seeded in 24-well plates and treated with pradimicin-IRD (1.25 μM, 2.5 μM and 5 μM) and doxorubicin (1 μM) for 48 h. Cells were then washed twice with ice cold PBS and resuspended in binding buffer containing 1 μg/mL 7AAD and 1 μg/mL APC-labeled annexin V (BD Biosciences, San Jose, CA, USA). All specimens were acquired by flow cytometry (FACSCalibur; Becton Dickinson, Lincoln Park, NJ, USA) after incubation for 15 min at room temperature in a light-protected area and analyzed using FlowJo software (Treestar, Inc., San Carlos, CA, USA).

2.8. Quantitative PCR

Total RNA from HCT 116 cells treated with pradimicin-IRD (5 μM) or doxorubicin (1 μM) was obtained using the TRIzol reagent (Thermo Fisher Scientific, San Jose, CA, USA). The cDNA was synthesized from 1 μg of RNA using a High-Capacity cDNA Reverse Transcription Kit (Thermo Fisher Scientific, San Jose, CA, USA). Quantitative PCR (qPCR) was performed with an ABI 7500 Sequence Detector System (Thermo Fisher Scientific, San Jose, CA, USA) with specific primers for *BCL2*, *BCL2L1*, *MCL1*, *BAX*, *BAD*, *BAK1*, *CCNA2*, *CCNB1*, *CCND1*, *CCNE1*, *CDKN1A* and *CDKN1B* (Integrated DNA Technologies – IDT, Coralville, Iowa, USA). Primer sequences are displayed in Table 1. The relative quantification value was calculated using the equation $2^{-\Delta\Delta CT}$ [7]. A negative 'No Template Control' was included for each primer pair.

2.9. Western blot

Equal amounts of protein were used as total extracts, followed by SDS-PAGE, Western blot analysis with the indicated antibodies and imaging using the SuperSignal™ West Dura Extended Duration Substrate System (Thermo Fisher Scientific, San Jose, CA, USA) and G: BOX Chemi XRQ (Syngene, Cambridge, UK). Antibodies against γH2AX (#9718), phospho (p)-Rb (#9308), Rb (#9309), cleaved PARP-1 (#5625), PARP1 (#9542), cleaved caspase-3 (#9604), caspase-3 (#9662), α-tubulin (#2144) and GAPDH (#5174) were obtained from Cell Signaling Technology (Danvers, MA, USA). Antibody against p21 (sc-6246) was obtained from Santa Cruz Biotechnology (Santa Cruz, CA, USA). Band intensities were determined using UN-SCAN-IT gel 6.1 software (Silk Scientific; Orem, UT, USA).

2.10. Mass spectrometry

The DNA binding study was developed according to a modified methodology described by Kelso et al. (2008). Double stranded DNA (dsDNA) (IDT, Coralville, Iowa, USA) was used, with the sequence 5′-TGCTCGGACG-3′ 3′-ACGAGCCTGC-5′. The oligonucleotides were dissolved in 100 mM of ammonium acetate (pH 7.5), held at 90 °C for 15 min and cooled slowly to room temperature to form the dsDNA. The stock solutions of 10 mM pradimicin-IRD and 10 mM doxorubicin in 100 mM of ammonium acetate (Sigma-Aldrich, St. Louis, MO, USA) (pH 7.5) were prepared. A mixture of dsDNA and pradimicin (1:10) was prepared containing 69 μL of 100 mM ammonium acetate (pH 7.5), 1 μL of dsDNA and 10 μL of stock solution of pradimicin-IRD. The mixture was allowed to equilibrate for 10 min and diluted by an addition of 120 μL of methanol to a final concentration of 50 mM dsDNA. Detection was performed by mass spectrometry (Bruker Daltonics, Billerica, MA, USA) fitted with an electrospray ionisation source and a Quadrupole-Time-of-Flight analyser [8]. The parameters employed were as follows: 2.8 kV of capillary energy, 220 °C capillary temperature, 5.0 Bar gas pressure, 450 V Endplate. A range of 1000–3000 Da was monitored during the negative ionisation mode.

2.11. Statistical analysis

Statistical analyses were performed using GraphPad Prism 5 (GraphPad Software, Inc.). For comparisons, the Student's *t*-test or the ANOVA test and Tukey's post-test were used. A p value of < 0.05 was considered statistically significant. All pairs were analysed, and statistically significant differences are indicated.

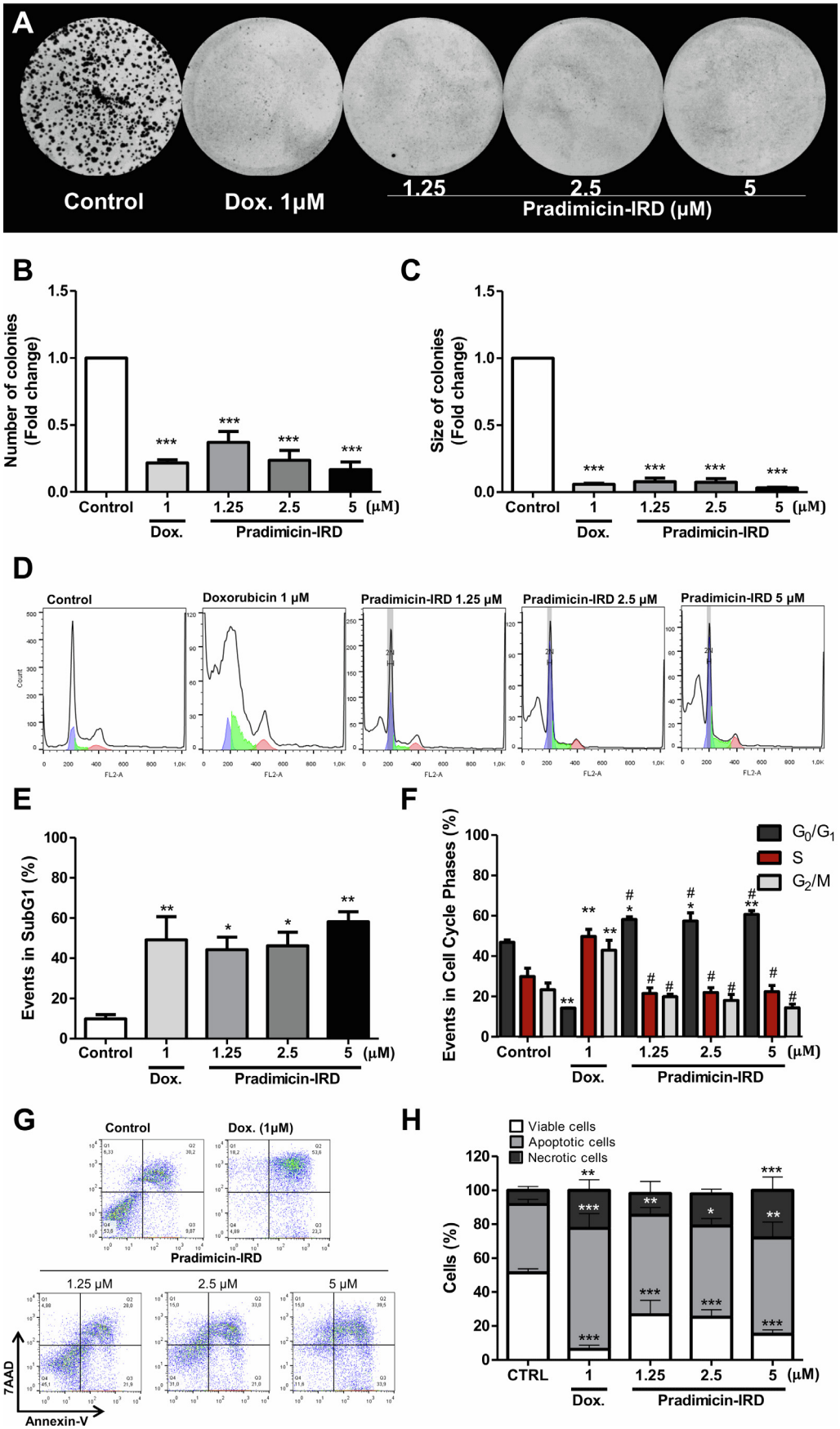

Fig. 2. Pradimicin-IRD reduces clonal growth and leads to cell arrest during the G_0/G_1 phase. Colony formation after pradimicin-IRD treatment for 6 h and placement in drug-free media for an additional 7 days. Representative images of colony formation after control (DMSO 0.05%), doxorubicin (1 μM) and pradimicin-IRD (1.25; 2.5 and 5 μM) treatment are illustrated (A). Bar graphs represent the number (B) and size (C) of colonies (mean ± SEM); ANOVA, one way, followed by Tukey's multiple comparison test, $^{**}p < 0.001$ $^{***}p < 0.0001$. Histograms represents $subG_1$, G_0/G_1, S and G_2/M cell populations in DMSO – (0.05%), doxorubicin – (1 μM) and pradimicin-IRD-treated cells (1.25; 2.5 and 5 μM) (D). Bar graphs represent the percentage of $subG_1$ cell population (E) and cell cycle distribution among the entire viable cell population (excluding subG1 cells) (n = 4) (mean ± SEM); ANOVA, one way, followed by Tukey's multiple comparison test, $^{*}p < 0.05$; $^{**}p < 0.01$; $^{\#}$ indicates parameters that are statistically significantly different from those of doxorubicin-treated cells ($p < 0.0001$) (F). Apoptosis was detected by flow cytometry in HCT 116 cells treated with doxorubicin (1 μM) and pradimicin-IRD (1.25 μM, 2.5 μM and 5 μM) for 48 h using an annexin V-FITC/7AAD staining method. Representative point graphs are shown for each condition; the upper and lower right quadrants (Q2 plus Q3) cumulatively contain the apoptotic population (annexin V + cells) (G). Annexin V positive HCT 116 cell percentages in doxorubicin (1 μM) and pradimicin-IRD (1.25 μM, 2.5 μM and 5 μM) treatments obtained by the 7AAD and annexin V-FITC labelled flow cytometry assay. Values expressed by mean and standard error of the mean (n = 3). The results are presented as mean ± SD of three independent experiments; * ($p < 0.01$); ** ($p < 0.001$); *** ($p < 0.0001$), ANOVA test and Tukey post-test, all pairs were analyzed and statistically significant differences are indicated (H).

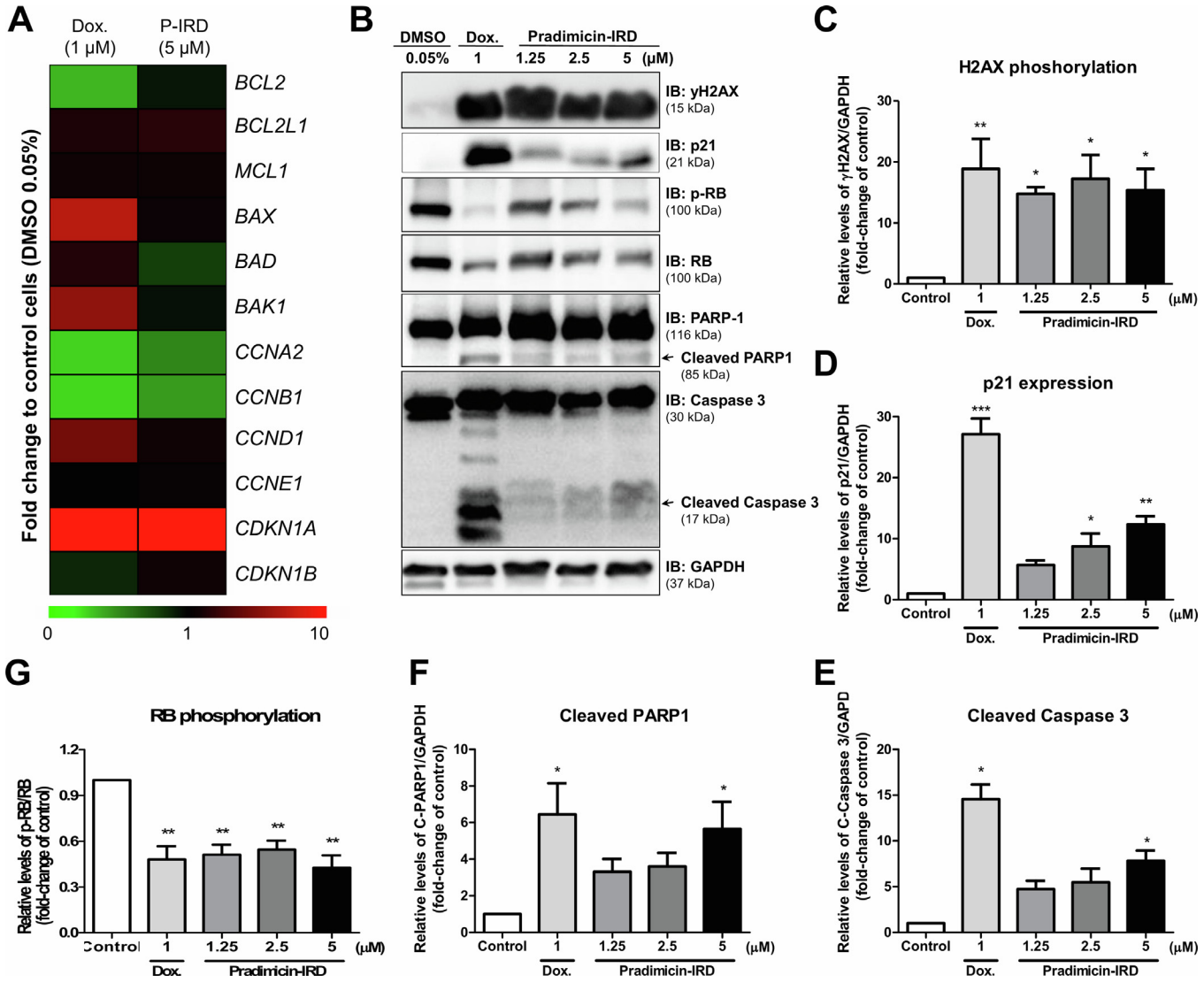

Fig. 3. Pradimicin-IRD induces DNA damage, cell cycle arrest and apoptosis markers in HCT 116 cells. The heatmap illustrates the quantitative polymerase chain reaction (qPCR) analysis of the *BCL2*, *BCL2L1*, *BAX*, *BAK1*, *CCNA2*, *CCNB1*, *CCND1*, *CCNE1*, *CDKN1A* and *CDKN1B* genes in HCT 116 cells after treatment with pradimicin-IRD (5 μM; mean; n = 3) or doxorubicin (1 μM; n = 1) for 48 h. Green and red indicate down and upregulated genes, respectively (A). Immunoblotting analysis for γH2AX, p21, phospho(p)-Rb, Rb, PARP-1, cleaved PARP-1, cleaved caspase3 and GAPDH of HCT 116 cells after incubation with DMSO (0.05%), doxorubicin (1 μM) and pradimicin-IRD (1.25; 2.5; and 5 μM) for 48 h (B). Pixel quantification of γH2AX (C), p21 (D), cleaved caspase-3 (E), cleaved PARP 1 (F), and pRb (G) (n = 3; mean ± SEM); ANOVA, one way, followed by Tukey's multiple comparison test, $^{*}p < 0.01$; $^{**}p < 0{,}001$; $^{***}p < 0.0001$. (For interpretation of the references to colour in this figure legend, the reader is referred to the web version of this article.)

3. Results

3.1. Pradimicin-IRD reduces cell viability

Pradimicin-IRD displayed a potential antitumoral activity with selectivity for colorectal carcinoma cell lines in comparison to primary fibroblast cell culture (Fig. 1A; Table 2). As HCT 116 *TP53*$^{+/+}$ presented the lowest mean inhibitory concentration (IC_{50}), it was the cell line chosen to the following studies. Pradimicin-IRD treatments promoted time-dependent cytotoxicity in HCT 116 cells (Fig. 1B). A pulse treatment of pradimicin-IRD for 6 h was sufficient to significantly reduce cell viability as measured after a total incubation time of 72 h (Fig. 1C). When the total incubation time was reduced to 24 h, even with continuous drug exposure, cytotoxic effects were reduced. Phenotypic effects of pradimicin-IRD are fully completed at least 48 h after the onset of the exposure, even when the compound was given as a pulse treatment of 6 h (Fig. 1C). Trypan blue staining results also show a significant decrease in total cells after pradimicin-IRD treatment (Fig. 1D). Both morphological analysis by haematoxylin-eosin staining and immunofluorescence showed a reduction of cell density and cell bodies after the pradimicin-IRD treatment, with condensation of the chromatin (Fig. 1E and F).

3.2. Pradimicin-IRD leads to reduced clonogenicity, G_0/G_1 cell cycle arrest and increased apoptosis

Pradimicin-IRD treatment resulted in a strong reduction of clonogenicity capacity after 6 h pulse treatment (Fig. 2A), as observed by the decreased number (Fig. 2B) and size (Fig. 2C) of colonies after 7 days. The cytotoxic potential of pradimicin-IRD was also confirmed by flow cytometry, which displayed a significant increase in $subG_1$ and annexin V positive cell populations, as well as decrease viable cell population, after pradimicin-IRD treatment for 48 h ($p < 0.05$; Fig. 2D, E and H). Regarding the cell cycle distribution among viable cell populations (excluding subG1 cells), pradimicin-IRD treatment induced a significant degree of G_0/G_1 cell cycle arrest ($p < 0.05$; Fig. 2D and F). A similar

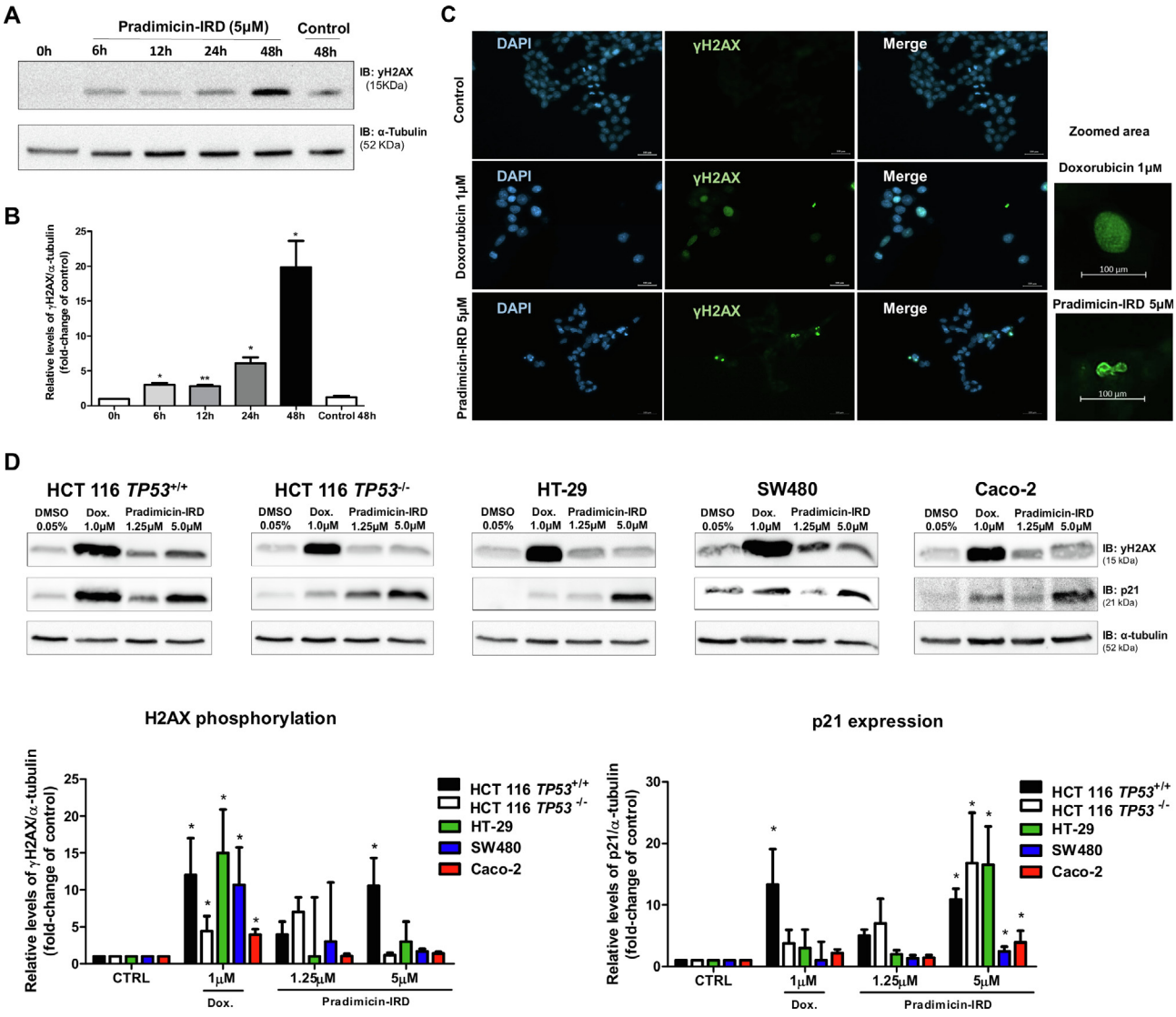

Fig. 4. Kinetics of pradimicin-IRD-induced DNA damage in HCT 116 cells. Immunoblotting of γH2AX and α-tubulin of HCT 116 cells after pradimicin-IRD (5 μM) treatment for 6, 12, 24 and 48 h (A). Bar graphs represent the quantification of three independent treatments (mean ± SEM); Student's *t* test, $^{*}p < 0.02$, $^{**}p < 0.009$ (B). Immunofluorescence of γH2AX and DAPI in HCT 116 cells after incubation with DMSO (0.05%) and pradimicin-IRD (5 μM) for 48 h (C). Immunoblotting analysis for γH2AX, p21 and α-tubulin of HCT 116 *TP53*$^{+/+}$, HCT 116 *TP53*$^{-/-}$, HT-29, SW480, and Caco-2 cells after incubation with DMSO (0.05%), doxorubicin (1 μM) and pradimicin-IRD (1.25; 2.5; and 5 μM) for 48 h. Pixel quantification of γH2AX and p21 (n = 3; mean ± SEM); ANOVA, one way, followed by Tukey's multiple comparison test, $^{*}p < 0.01$ (D).

phenomenon was confirmed after 24 h of pradimicin-IRD treatment (data not shown).

3.3. Molecular markers of DNA damage, cell cycle arrest and apoptosis are upregulated by pradimicin-IRD

In order to obtain novel insights about the molecular mechanisms involved in pradimicin-IRD response, we evaluated key genes involved in cell cycle progression and apoptosis. Among the genes evaluated in HCT 116 cells undergoing pradimicin-IRD treatment, the following changes were observed: *CDKN1A* (p21) mRNA levels increased, whereas *CCNA2* (cyclin A2) and *CCNB1* (cyclin B1) mRNAs levels decreased (Fig. 3A). Protein expression/activation analysis demonstrated a reduction in phospho (p)-Rb and increased levels of DNA damage markers (γH2AX and p21) and apoptosis markers (cleaved PARP1 and cleaved caspase 3). (Fig. 3B–G). A kinetics analysis of pradimicin-IRD treatment indicated that 6 h of drug exposure was sufficient to induce γH2AX expression in HCT 116 cells (Fig. 4A and B), corroborating the results observed in the cell viability and clonal growth assays. The induction of γH2AX by pradimicin-IRD was also confirmed by immunofluorescence after 48 h of treatment (Fig. 4C). The increased expression of p21 was observed in all tested colorectal carcinoma cell lines after pradimicin-IRD treatments. However, γH2AX expression was unchanged in *TP53* mutated cell lines (Fig. 4D).

3.4. Molecular interactions between pradimicin-IRD and DNA

Finally, mass spectrometry of DNA binding analysis indicated that pradimicin-IRD (2 molecules) is able to interact with double stranded DNA (Fig. 5). However, whereas doxorubicin was able to interact with the FOAT sequence as 1 and 2 molecules, only FOAT with 2 molecules of pradimicin-IRD was observed. This result shows that pradimicin-IRD and DNA molecules are able to interact with each other, which means that DNA might be a target for pradimicin-IRD.

4. Discussion

Pradimicin-IRD is a natural polycyclic antibiotic with cytotoxic

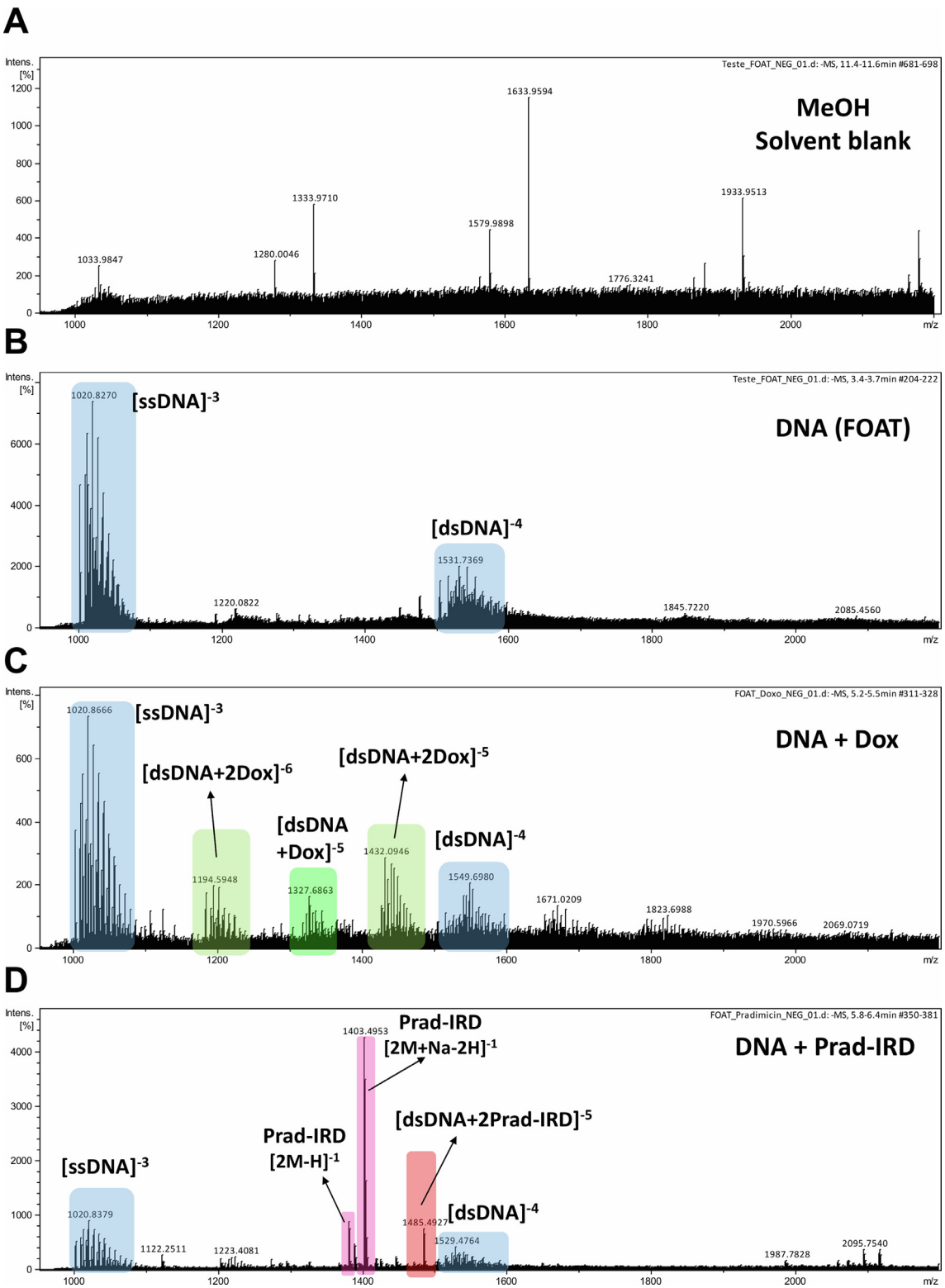

Fig. 5. Pradimicin-IRD binds to DNA. DNA-binding study by mass spectrometry (ESI-) of the FOAT DNA sequence with doxorubicin or pradimicin-IRD. Methanol (solvent blank) (A); FOAT (negative control) (B); FOAT:Doxorubicin (1:10) (positive control) (C); FOAT:pradimicin-IRD (1:10) (D).

activity against cancer cell lines, including MM 200 (melanoma, IC_{50} 2.7 μM), MCF-7 (breast carcinoma, IC_{50} 1.55 μM) and HCT 116 (IC_{50} 0.8 μM) [5]. Herein the anticancer potential of Pradimicin-IRD was further evaluated in a panel of colorectal cancer cells with different mutation status of cancer critical genes. The colorectal carcinoma cell lines represent the heterogeneity of colon cancer patients, where the most common mutated genes included the proto-oncogene *KRAS* (**wide type:** SW480 and Caco-2; **mutated:** HCT 116, HCT 116 *TP53*$^{-/-}$ and HT-29) and the tumor suppression gene *TP53* (**wide type:** HCT 116; **mutated:** HCT 116 *TP53*$^{-/-}$, SW480 and Caco-2HT-29), along with microsatellite instability and CpG island methylator phenotype [9]. Pradimicin-IRD was equally active against all tested colon cancer cells,

but significantly less toxic to a non-tumor primary fibroblast, suggesting selectivity to tumor cells in spite of the mutation status. Due to the sensitivity of the HCT 116 cell line to the drug, this cell line was selected for further investigation. Pradimicin-IRD displayed antitumor activity in HCT 116 cells with IC_{50} at the micromolar level and effects occurring after at least 6 h pulse treatment, and lasting several days, as demonstrated by the MTT (72 h) and clonogenic (7 days) assays. This information is particularly important from the translational point of view, since extrapolation into the clinical setting, 6 h of plasma life or infusion time is sufficient to achieve a long-term therapeutic effect.

Pradimicins are produced mainly by the bacteria from the genus *Actinomadura*, and their molecular structure is characterised by an aglycone dihydrobenzo (α) naphthoquinone with D-amino acid and hexose substitutions [10]. Previous studies have highlighted the antifungal and antiviral properties of pradimicins [11–14]. However, the antitumor activity of pradimicins is rarely discussed [15,16]. Thus, the mechanism of action of a novel derivative of pradimicin (i.e., pradimicin-IRD) that has presented a potential unexplored anticancer activity should be elucidated.

In the molecular scenario, we determined that pradimicin-IRD binds to DNA, induces DNA damage and the activation of genes/proteins that lead to cell cycle arrest, including γH2AX and p21 (*CDKN1A*). γH2AX, the phosphorylated form of histone H2AX at serine 139, is a well-established DNA damage marker; it is mainly phosphorylated by the mutated ataxia telangiectasia (ATM) protein [17,18]. *CDKN1A* gene expression is activated by p53 as a result of ATM activation, promoting cell cycle arrest at the G1 phase via inhibition of CDK-cyclin complexes [19]. Indeed, we observed increased levels of p21 mRNA and protein and decreased levels of cyclin A2 (*CCNA2*) and cyclin B1 (*CCNB1*) mRNA in pradimicin-IRD treated-cells. CDK2-cyclin E complex, for example, promotes Rb phosphorylation and E2F release for the transcription of pro-proliferative factors, such as the *cyclin A2* (*CCNA2*) gene [20]. Pradimicin-IRD decreases the levels of Rb phosphorylation, which may be the cause of G_0/G_1 cell cycle arrest.

The pradimicin-IRD treatment in *TP53* mutated cell lines displayed, unlikely doxorubicin treatments, a p53-independent regulation of p21 expression. Further investigation of the alternative pathway of p21 activation would be important, such as CHEK2-dependent senescence and/or BRCA1 induction [21,22], since the selectivity was not impacted by different cancer cell mutational background. This result positively influenced the translational potential of pradimicin-IRD.

The current DNA-damaging agents used in the clinical setting are most cytotoxic during the S-phase, leading to G_2/M cell cycle arrest. For instance, cisplatin forms 1, 2-intrastrand cross-links of adjacent deoxyguanosines with platinum binding to the N7 positions of the DNA bases [23,24]. Inhibitors of topoisomerase (e.g., doxorubicin) form a DNA-enzyme complex, preventing the re-ligation of DNA strands and causing toxic double-strand breaks. Compounds that cause these lesions are potent inhibitors of DNA replication, which could induce G_2/M phase cell cycle arrest, which differs from pradimicin-IRD induced G_0/G_1 cell cycle arrest. However, pradimicin-IRD promotes a decrease in S-phase cell populations, indicating that the DNA damage caused by pradimicin-IRD occurs prior to the DNA synthesis. Although the identification of the biochemical molecular target can be difficult due to the many complex cellular processes involved within the cell, our results from DNA-binding assays via mass spectrometry show that pradimicin-IRD is able to bind DNA, as well as doxorubicin and chromomycin A3, well-known DNA-binding compounds. There are many examples in the literature of DNA-binding investigation by ESI-MS [25–28]. Such assays became routine in our research group because they are simple and fast to perform. For instance, in a previous study, we demonstrated the ability of the anthracyclines nocardicyclin and nothramycin to bind dsDNA (FOAT) [8]. Although dsDNA with only 1 molecule was detected for both anthracyclines, it is interesting that for doxorubicin and pradimicin-IRD, we detected dsDNA with 2 molecules. These results indicate that the interaction is related to the chemical structure since pradimicin has the same aminoglycoside of nocardicyclin and nothramycin, suggesting that the number of molecules able to bind this DNA sequence is correlated with the aglycone moiety. Still, it is known that chromomycin A3, a penta-glycoside anthraquinone, complex with a DNA sequence consisting of a dimer of 2 molecules in coordination with a Mg^{2+} [29]; therefore, our results may also indicate that pradimicin interacts with DNA as a dimer of 2 molecules. The first-line treatment for colorectal cancer [30] is mainly based on combinations of DNA-damaging agents, such as oxaliplatin, a third-generation platinum compound; 5-fluorouracil (5-FU) and capecitabin, pyrimidine analogues that inhibit DNA synthesis; and irinotecan, a topoisomerase inhibitor [31,32]. DNA-damaging agents are widely used in cancer therapy, but their use is limited by dose-related toxicities, as well as the development of drug resistance. Studies related to new information about the DNA damage response network and its role in drug discovery are essential to overcome these problems and offer novel therapeutic options [3,33].

In summary, cellular and molecular analyses indicate that pradimicin-IRD induced DNA damage, cell cycle arrest and apoptosis in a colorectal carcinoma cell line (HCT 116). Our exploratory study identified novel targets for pradimicin-IRD and provided insights concerning its potential anticancer activity.

Acknowledgements

The authors are grateful to Coordenação de Aperfeiçoamento de Pessoal de Nível Superior – Brasil (CAPES – Finance Code 001), National Council for Scientific and Technological Development – Brasil (CNPq, grants # 421124/2016-4; 402587/2016-2) and São Paulo Research Foundation (FAPESP grants # 2018/17595-0; 2017/17648-4; 2017/24993-0; 2015/17177-6) for funding allotted for the execution of this work. The authors also acknowledge financial support from the National Institute of Science and Technology – INCT BioNat, (CNPQ grant # 465637/2014-0, FAPESP grant # 2014/50926-0, Brazil).

Declaration of Competing Interest

The authors declare no competing financial interests.

References

[1] D. Branzei, M. Foiani, Regulation of DNA repair throughout the cell cycle, Nat. Rev. Mol. Cell Biol. 9 (2008) 297–308.
[2] C.J. Lord, A. Ashworth, The DNA damage response and cancer therapy, Nature 481 (2012) 287–294.
[3] K. Cheung-Ong, G. Giaever, C. Nislow, DNA-damaging agents in cancer chemotherapy: serendipity and chemical biology, Chem. Biol. 20 (2013) 648–659.
[4] L.H. Pearl, A.C. Schierz, S.E. Ward, B. Al-Lazikani, F.M. Pearl, Therapeutic opportunities within the DNA damage response, Nat. Rev. Cancer 15 (2015) 166–180.
[5] A. Bauermeister, F.A. Calil, C.L.P.F. das, T.C.T. Medeiros, L.C. Almeida, L.J. Silva, I.S. de Melo, T.D. Zucchi, L.V. Costa-Lotufo, L.A.B. Moraes, Pradimicin-IRD from *Amycolatopsis* sp. IRD-009 and its antimicrobial and cytotoxic activities, Nat. Prod. Res. (2018) 1–8.
[6] T. Mosmann, Rapid colorimetric assay for cellular growth and survival: application to proliferation and cytotoxicity assays, J. Immunol. Methods 65 (1983) 55–63.
[7] K.J. Livak, T.D. Schmittgen, Analysis of relative gene expression data using real-time quantitative PCR and the 2(-Delta Delta C(T)) method, Methods 25 (2001) 402–408.
[8] A. Bauermeister, T.D. Zucchi, L.A. Moraes, Mass spectrometric approaches for the identification of anthracycline analogs produced by actinobacteria, J. Mass Spectrom. 51 (2016) 437–445.
[9] D. Ahmed, P.W. Eide, I.A. Eilertsen, S.A. Danielsen, M. Eknaes, M. Hektoen, G.E. Lind, R.A. Lothe, Epigenetic and genetic features of 24 colon cancer cell lines, Oncogenesis 2 (2013) e71.
[10] T.J. Walsh, N. Giri, Pradimicins: a novel class of broad-spectrum antifungal compounds, Eur. J. Clin. Microbiol. Infect. Dis. 16 (1997) 93–97.
[11] T. Ueki, K. Numata, Y. Sawada, T. Nakajima, Y. Fukagawa, T. Oki, Studies on the mode of antifungal action of pradimicin antibiotics. I. Lectin-mimic binding of BMY-28864 to yeast mannan in the presence of calcium, J. Antibiot. (Tokyo) 46 (1993) 149–161.
[12] F.J. van der Meer, C.A. de Haan, N.M. Schuurman, B.J. Haijema, M.H. Verheije, B.J. Bosch, J. Balzarini, H.F. Egberink, The carbohydrate-binding plant lectins and the non-peptidic antibiotic pradimicin A target the glycans of the coronavirus

envelope glycoproteins, J. Antimicrob. Chemother. 60 (2007) 741–749.
[13] Y. Nakagawa, T. Doi, T. Taketani, K. Takegoshi, Y. Igarashi, Y. Ito, Mannose-binding geometry of pradimicin A, Chemistry 19 (2013) 10516–10525.
[14] T. Doi, Y. Nakagawa, K. Takegoshi, Solid-state nuclear magnetic resonance analysis reveals a possible calcium binding site of pradimicin A, Biochemistry 56 (2017) 468–472.
[15] T. Oki, Y. Yamazaki, T. Furumai, Y. Igarashi, Pradimicin, a mannose-binding antibiotic, induced carbohydrate-mediated apoptosis in U937 cells, Biosci. Biotechnol. Biochem. 61 (1997) 1408–1410.
[16] T. Oki, Y. Yamazaki, N. Nomura, T. Furumai, Y. Igarashi, Involvement of Ca2+ ion and reactive oxygen species as a mediator in pradimicin-induced apoptosis, J. Antibiot. (Tokyo) 52 (1999) 455–459.
[17] E.P. Rogakou, D.R. Pilch, A.H. Orr, V.S. Ivanova, W.M. Bonner, DNA double-stranded breaks induce histone H2AX phosphorylation on serine 139, J. Biol. Chem. 273 (1998) 5858–5868.
[18] S. Burma, B.P. Chen, M. Murphy, A. Kurimasa, D.J. Chen, ATM phosphorylates histone H2AX in response to DNA double-strand breaks, J. Biol. Chem. 276 (2001) 42462–42467.
[19] A.G. Georgakilas, O.A. Martin, W.M. Bonner, p21: a two-faced genome guardian, Trends Mol. Med. 23 (2017) 310–319.
[20] A.P. Bracken, M. Ciro, A. Cocito, K. Helin, E2F target genes: unraveling the biology, Trends Biochem. Sci. 29 (2004) 409–417.
[21] C.M. Aliouat-Denis, N. Dendouga, I. Van den Wyngaert, H. Goehlmann, U. Steller, I. van de Weyer, N. Van Slycken, L. Andries, S. Kass, W. Luyten, M. Janicot, J.E. Vialard, p53-independent regulation of p21Waf1/Cip1 expression and senescence by Chk2, Mol. Cancer Res. 3 (2005) 627–634.
[22] A.L. Gartel, A.L. Tyner, Transcriptional regulation of the p21((WAF1/CIP1)) gene, Exp. Cell Res. 246 (1999) 280–289.
[23] J.N. Burstyn, W.J. Heiger-Bernays, S.M. Cohen, S.J. Lippard, Formation of cis-diamminedichloroplatinum(II) 1,2-intrastrand cross-links on DNA is flanking-sequence independent, Nucl. Acids Res. 28 (2000) 4237–4243.
[24] Y. Liu, B.K. Law, H. Luesch, Apratoxin a reversibly inhibits the secretory pathway by preventing cotranslational translocation, Mol. Pharmacol. 76 (2009) 91–104.
[25] V.E. Reeve, G.E. Greenoak, P.J. Canfield, C. Boehm-Wilcox, C.H. Gallagher, Topical urocanic acid enhances UV-induced tumour yield and malignancy in the hairless mouse, Photochem. Photobiol. 49 (1989) 459–464.
[26] C. Kelso, V. Tillott, J.D. Rojas, R.L. Furlan, G. Padilla, J.L. Beck, Mass spectrometric investigation of the DNA-binding properties of an anthracycline with two trisaccharide chains, Arch. Biochem. Biophys. 477 (2008) 348–355.
[27] K.M. Keller, J. Zhang, L. Oehlers, J.S. Brodbelt, Influence of initial charge state on fragmentation patterns for noncovalent drug/DNA duplex complexes, J. Mass Spectrom. 40 (2005) 1362–1371.
[28] F. Rosu, S. Pirotte, E. De Pauw, V. Gabelica, Positive and negative ion mode ESI-MS and MS/MS for studying drug–DNA complexes, Int. J. Mass Spectrom. 253 (2006) 156–171.
[29] M.H. Hou, H. Robinson, Y.G. Gao, A.H. Wang, Crystal structure of the [Mg2+-(chromomycin A3)2]-d(TTGGCCAA)2 complex reveals GGCC binding specificity of the drug dimer chelated by a metal ion, Nucl. Acids Res. 32 (2004) 2214–2222.
[30] M.G. Brattain, W.D. Fine, F.M. Khaled, J. Thompson, D.E. Brattain, Heterogeneity of malignant cells from a human colonic carcinoma, Cancer Res. 41 (1981) 1751–1756.
[31] E.J. Kuipers, W.M. Grady, D. Lieberman, T. Seufferlein, J.J. Sung, P.G. Boelens, C.J. van de Velde, T. Watanabe, Colorectal cancer, Nat. Rev. Dis. Primers 1 (2015) 15065.
[32] R.M. McQuade, V. Stojanovska, J.C. Bornstein, K. Nurgali, Colorectal cancer chemotherapy: the evolution of treatment and new approaches, Curr. Med. Chem. 24 (2017) 1537–1557.
[33] K. Fujita, Y. Kubota, H. Ishida, Y. Sasaki, Irinotecan, a key chemotherapeutic drug for metastatic colorectal cancer, World J. Gastroenterol. 21 (2015) 12234–12248.